Tuning Magnetic Chirality by Dipolar Interactions

Juriaan Lucassen,* Mariëlle J. Meijer, Oleg Kurnosikov, Henk J. M. Swagten, Bert Koopmans, and Reinoud Lavrijsen
Department of Applied Physics, Eindhoven University of Technology, P.O. Box 513, 5600 MB Eindhoven, Netherlands

Fabian Kloodt-Twesten and Robert Frömter
Universität Hamburg, Center for Hybrid Nanostructures, Luruper Chaussee 149, 22761 Hamburg, Germany

Rembert A. Duine
Department of Applied Physics, Eindhoven University of Technology, P.O. Box 513, 5600 MB Eindhoven, Netherlands and Institute for Theoretical Physics, Utrecht University, Leuvenlaan 4, 3584 CE Utrecht, Netherlands

(Received 6 June 2019; published 11 October 2019)

The stabilization of chiral magnetic domain walls and skyrmions has been attributed to the actively investigated Dzyaloshinskii-Moriya interaction. Recently, however, predictions were made that suggest dipolar interactions can also stabilize chiral domain walls and skyrmions, but direct experimental evidence has been lacking. Here we show that dipolar interactions can indeed stabilize chiral domain walls by directly imaging the magnetic domain walls using scanning electron microscopy with polarization analysis in archetype Pt/CoB/Ir thin film multilayers. We further demonstrate the competition between the Dzyaloshinskii-Moriya and dipolar interactions by imaging a reversal of the domain wall chirality as a function of the magnetic layer thickness. Finally, we suggest that this competition can be tailored by a Ruderman-Kittel-Kasuya-Yosida interaction. Our work therefore reveals that dipolar interactions play a key role in the stabilization of chiral spin textures. This insight will open up new routes towards balancing interactions for the stabilization of chiral magnetism.

DOI: 10.1103/PhysRevLett.123.157201

The role of chirality is becoming more important for new applications in spintronics, especially in ultrathin magnetic films [1–6]. In magnetic racetrack applications, for example, the chirality directly determines how magnetic domain walls and skyrmions interact with the spin-orbit torques [2,3,7–10]. It is therefore important to investigate the key contributing factors to this chirality. The underlying interaction that is believed to stabilize the chirality is the Dzyaloshinskii-Moriya interaction (DMI). As shown by a wealth of theoretical and experimental reports this interaction requires the breaking of inversion symmetry and originates from the interface between a heavy metal and a ferromagnet for the thin film systems investigated in this Letter [4,11]. The DMI also helps to stabilize skyrmions because it favors noncollinear spin configurations [12], which are envisaged to be used in areas ranging from magnetic racetrack memory and logic applications, to radio frequency devices and neuromorphic computing [5,6].

Very recently, however, it was realized that DMI is not the only interaction that can stabilize a specific chirality [8–10,13–15]. Actually, already 40 years ago it was shown that the presence of dipolar fields leads to the formation of chiral Néel caps [16,17]. Here, the stray fields originating from magnetic domains align the spins inside the domain walls at the top of the film to form clockwise (CW) Néel walls and at the bottom of the film to form counterclockwise (CCW) Néel walls, providing an optimized flux closure state. Dipolar interactions can often be ignored for thin-film systems used in domain-wall studies. This is no longer the case for the multilayer repeat systems often used to stabilize room-temperature magnetic skyrmions because of the increase in magnetic volume and reduced coupling across the nonmagnetic spacer layers [15–19].

Recently, theoretical studies [8–10,13,20] have shown that without DMI indeed multilayered systems exhibit two Néel caps with opposite chirality. Including DMI, however, leads to a larger fraction of the layers being occupied by the Néel cap of the chirality favored by the DMI. The other cap will be reduced in size and occupy fewer layers. This happens until the DMI is so large that it is no longer energetically favorable to accommodate a Néel cap not favored by the DMI and a homochiral domain wall is formed. The energetics and dynamics of both skyrmions and domain walls are affected by this competition because it determines the net chirality of the magnetic textures, which in turn influences the interaction with, for example, spin-orbit torques [8–10]. It is therefore vital to experimentally confirm these predictions. Observations reported in Refs. [13,14] suggest the presence of Néel caps based on measurements of the magnetic stray fields. Another study

directly measures the domain-wall chirality across a range of systems and finds one stack out of many where the domain-wall chirality appears to be determined by the dipolar interactions [8]. Hence, unambiguous experimental verification of the predicted domain-wall behavior has proven to be extremely challenging because it is very difficult to image magnetic domain walls directly. Here, we present systematic experiments confirming the proposed competition between the effective DMI, characterized by the constant D, and dipolar interactions for the formation of chiral magnetic domain walls.

We do this by directly imaging the magnetic domain-wall texture in the top CoB layer of an archetype multilayered system of //Ta(4)/Pt(2)/[Pt(1)/$Co_{80}B_{20}$(0.7)/Ir(1)]x6/Pt(1)/$Co_{80}B_{20}$(t) (thicknesses in parentheses in nm) using an *in situ* scanning electron microscope with polarization analysis (SEMPA) [21]. By wedging the top layer such that t varies continuously between 0.7 and 1.4 nm we access a regime of low and high effective D in a single layer due to the interfacial nature of the DMI, originating from the Pt/CoB interface, yet leave the dipolar fields from the bottom repeats unaffected. We find that going from low (<1.1 nm) to high (>1.1 nm) CoB thicknesses the domain-wall chirality reverses from CCW Néel to CW Néel as the effective DMI decreases with respect to the dipolar interactions. We elucidate the physical interactions at play using a combination of a simple analytical model and micromagnetic simulations. Additionally, we argue that a small indirect (asymmetric [22]) exchange interaction, known as the Ruderman-Kittel-Kasuya-Yosida (RKKY) interaction, that couples magnetic layers across a nonmagnetic spacer can tailor the competition between the dipolar interaction and the DMI [23].

A SEMPA measurement on a CoB thickness of $t =$ 1.2 nm is shown in the two frames of Fig. 1(a). The two images show the m_y and m_x magnetization components imaged simultaneously on the same area, where both images also contain OOP (m_z) contrast. There are two main features in the m_y image. First, a wormlike domain pattern given by the OOP domains. Second, a dark lining on top of the light domains, and a bright lining on the bottom of the light domains, which correspond to the domain walls. This lining is not present on the left and right of the domains, which suggests these are Néel walls. In the m_x measurement the linings are on the left and right side of the OOP domains. We can combine both the OOP and IP information from both images to form a composite image [31,32] which is shown in Fig. 1(b).

Here, the OOP domains are shown in white and black, inferred from the contrast in the m_y image. Superimposed, we show the domain walls where the direction of the magnetization inside the domain walls is indicated in color following the color wheel. By looking at several walls one finds that in most walls the magnetization points from the up to the down domains. To quantify this further,

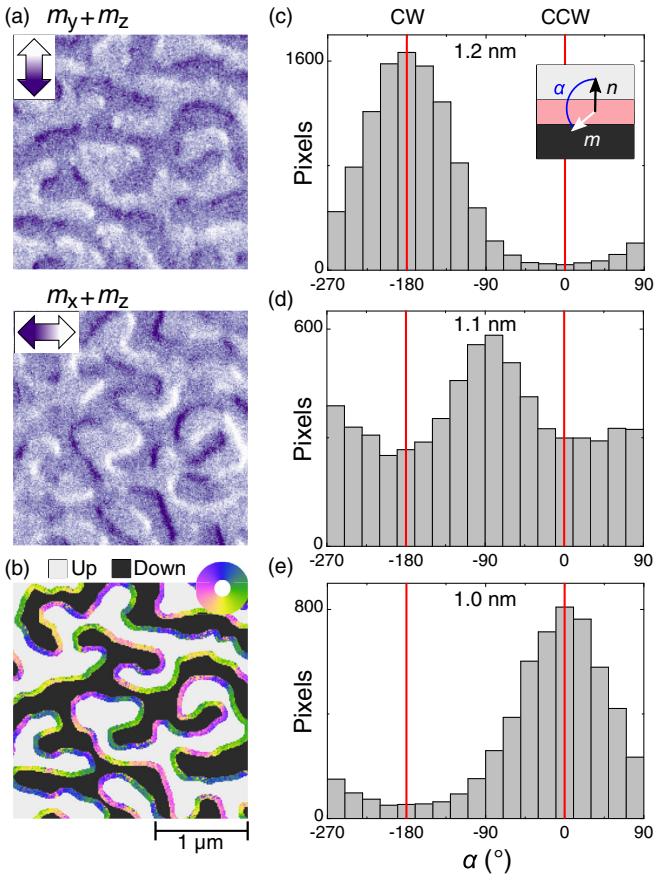

FIG. 1. (a) SEMPA measurements (scale bar at bottom) for $t = 1.2$ nm. From top to bottom: 1. m_y + OOP contrast (m_z), 2. m_x + OOP contrast (m_z). The arrows indicate the direction of the magnetization contrast. (b) Composite image constructed from (a). The OOP domains are indicated in black and white and the in-plane magnetic domain wall is shown in color, with the color corresponding to the direction of the magnetization in the wall as given by the color wheel. (c)–(e) Histograms of the domain-wall angle α for $t = 1.2$, 1.1, and 1.0 nm, respectively. These histograms are for all pixels in the domain wall, where $\alpha = 0, -180°$ indicates a CCW and CW Néel wall, respectively. The definition of the domain-wall angle α between the domain-wall normal n and the magnetization inside the domain wall m is given in the inset of (c).

we construct a histogram of the domain-wall angle α between the domain-wall normal n and the domain-wall magnetization m which is shown in Fig. 1(c) (inset gives definition of α). This histogram is sharply peaked around $\alpha = -180°$ which indicates that CW Néel walls dominate at this thickness. The full width at half maximum (FWHM) of the histogram could be used to determine the spread in domain-wall angles. However, we estimate that the dominating contribution to the FWHM of the histogram is the result of Poisson noise in the electron counting [33] and errors in the determination of the domain-wall normal (see Supplemental Material [23], Sec. V) [31]. We therefore give no quantitative estimation of the spread in

domain-wall angles, but we know it to be much smaller than the histogram width.

In the other two histograms of Fig. 1 we show the domain-wall distributions obtained in a similar matter for $t = 1.1$ [Fig. 1(d)] and 1.0 nm [Fig. 1(e)]. For $t = 1.0$ nm the domain-wall chirality has reversed and the corresponding histogram is now peaked around a CCW Néel wall orientation ($\alpha = 0°$). For $t = 1.1$ nm there is a transition region with different types of domain walls. From the histogram we conclude that there is slight preference for achiral Bloch walls based on the minimal peaks shown at $\alpha = \pm 90°$ [34]. This transition from homochiral CW Néel walls at 1.2 nm to CCW Néel walls at 1.0 nm is the result of dipolar interactions that are in direct competition with the DMI. Below 1.1 nm the DMI dominates (favoring CCW Néel walls) whereas dipolar interactions dominate above 1.1 nm (preferring CW Néel walls). Raw data belonging to the other two histograms as well as additional measurements for different thicknesses on the same sample and similar measurements on a nominally identical sample can be found in the Supplemental Material [23], Sec. II.

To substantiate the observations, in what follows we will use a simple analytical model to explain our results. The fundamentals of this model, adapted from Ref. [8], are given in Fig. 2(a), where we show a CoB layer with a CCW Néel wall on top of a multilayer stack and the effective IP magnetic fields acting on the domain wall in this top CoB layer. In the original model of Ref. [8] there are two in-plane magnetic fields that determine if the CCW domain-wall chirality assumed in the top CoB layer is the stable configuration. First, the dipolar field from the stack underneath. Second, an effective field from the DMI of the top CoB layer itself. We add to this model a third term: a RKKY interaction as Ir is a well-known RKKY mediating layer [35] whose coupling can persist through thin layers of Pt [36]. This term is often overlooked but can be of significant importance as we demonstrate later in this Letter. We assume that the underlying layers of thickness 0.7 nm contain CCW Néel walls induced by the DMI ($D > 0$), because the experiments consistently show CCW Néel walls below 1.1 nm (see Supplemental Material [23], Sec. II). To figure out if this assumed CCW Néel wall is the lowest-energy domain-wall type, we use analytical expressions derived in the Supplemental Material [23], Sec. IV, based on derivations presented elsewhere, to calculate the dipolar and DMI fields [8,37]. The details on the calculations for the added RKKY field are also presented in the Supplemental Material [23], Sec. IV.

These calculated magnetic fields are shown in Fig. 2(b) for an antiferromagnetic ($J < 0$) RKKY interaction. Apart from the strength of D and J, which we vary, all other input parameters are based on the experimental parameters of the investigated system. The DMI field points in the $+x$ direction (>0), indicating a preference for CCW Néel walls. However, the dipolar and RKKY field point from

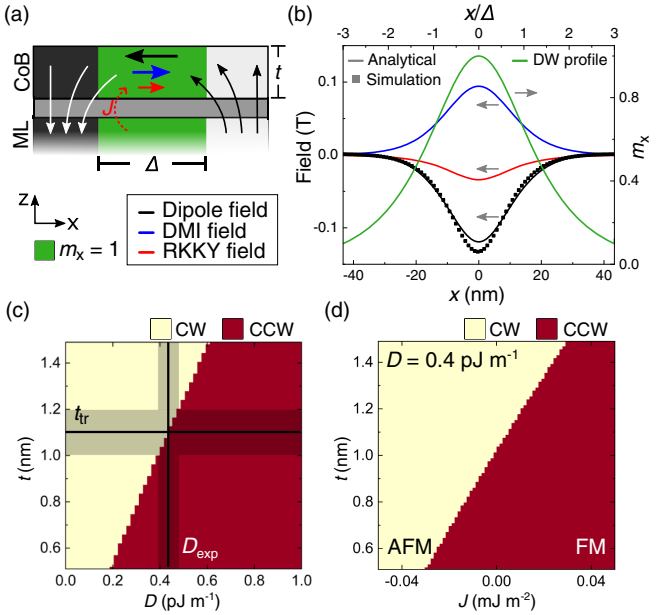

FIG. 2. (a) Basics of the model. A CoB layer on top of a multilayer (ML) stack with CCW Néel walls indicated in green with the 3 effective IP magnetic fields acting on the domain wall in this layer indicated by the arrows. (b) Magnitude of the effective fields (black, blue, and red are the dipolar, DMI, and RKKY fields, respectively; left axis) in the x direction, including the domain-wall profile (green; right axis), as a function of position. Plotted are the analytical results as well as the resulting dipolar field from micromagnetic simulations for $t = 1.2$ nm, $J = -0.02$ mJ m^{-2}, and $D = 0.4$ pJ m^{-1}. (c),(d) Phase diagrams according to the analytical model for the domain-wall chirality in the top CoB layer as a function of (c) D and t with $J = 0$ mJ m^{-2} and (d) J and t for $D = 0.4$ pJ m^{-1}. In (c), the black area indicates the experimental thickness transition region t_{tr} and DMI D_{exp}.

the up domain towards the down domain and are thus directed in the opposite ($-x$) direction favoring CW Néel walls. The sum of these magnetic fields integrated across the domain-wall profile [also indicated in Fig. 2(b)] determines whether the assumed CCW profile is favored [8]. In this example, the dipolar fields are dominant (total integrated field points in the $-x$ direction) and the resulting domain-wall profile of the top CoB layer will be CW rather than the assumed CCW wall.

Comparing the values of the integrated magnetic fields as a function of t and D for a situation without RKKY coupling yields the phase plot depicted in Fig. 2(c), where we plot the resulting domain-wall chirality of the top CoB layer as a function of both parameters. With increasing t the effective DMI field reduces as $1/t$ due to its interfacial nature, until it is so small that the dipolar interactions become dominant and the top domain wall is of the CW Néel type. However, if we include the RKKY interaction the situation is modified as we demonstrate in Fig. 2(d), where the domain-wall chirality is shown as a function of both t and J for $D = 0.4$ pJ m^{-1}. Apparently, the transition

thickness from CW to CCW can be shifted as a function of the RKKY interaction, where it shifts to thicker layers for ferromagnetic ($J > 0$) coupling and to thinner layers for antiferromagnetic ($J < 0$) coupling. As this effect occurs for reasonably small values of J [35,36] we conclude that an independent quantification of both J and D is not possible when both interactions are present.

We demonstrate in Supplemental Material [23], Sec. VI that for our samples the RKKY coupling is $|J| < 0.001$ mJ m^{-2}. Following the phase diagram, we then find that its influence is negligible and that we can use Fig. 2(c) to determine the DMI. As found above, the transition thickness t_{tr} between CW and CCW Néel walls is between 1.0 and 1.2 nm experimentally. Based on these elementary model calculations we therefore conclude that the experimental DMI D_{exp} is $+0.44 \pm 0.05$ pJ m^{-1} (indicated by the black lines in the figure) for the top Pt/CoB interface [38]. This value is slightly lower than reported for Pt/Co, Pt/CoFeB and Pt/$Co_{68}B_{32}$ interfaces, which is around $+1$ pJ m^{-1} [39].

Although our simple interpretation using this elementary model describes our observations quite well, two issues need to be carefully addressed. First, for these calculations we assumed the domain-wall width to be constant as a function of t and matched it to a micromagnetic simulation for the parameters of Fig. 2(b). Yet, we know this width to be thickness dependent through the effective anisotropy K_{eff} and complex interactions with the dipolar fields. Second, the model does not suggest the presence of Bloch domain walls which is what we observe experimentally at $t = 1.1$ nm. To tackle these issues we derived a more complete picture by performing micromagnetic simulations where we simulate the complete system and look at its influence on the chirality of the domain walls in the top CoB layer. Using this approach, the variation in the domain-wall width and possible presence of a Bloch wall is taken into account.

In Figs. 3(a) and 3(b) we show cross sections of the magnetic texture determined using micromagnetic simulations, where the domain walls in the bottom repeats are aligned along the CCW direction favored by the DMI (which was assumed implicitly for the analytical calculations). However, in (a) due to the increased thickness (1.2 nm) of the top layer the effective DMI of that layer is not strong enough to overcome the dipolar interactions, resulting in a CW Néel wall for the top CoB layer. In (b) the top layer is thinner (0.8 nm) and now the effective DMI is dominant. Running these simulations for different D and t and extracting the resulting top domain-wall angle α produces Fig. 3(c). We find behavior akin to Fig. 2(c), where the domain-wall chirality reverses between CCW ($\alpha = 0°$) and CW ($\alpha = 180°$) as a function of D and t. Additionally, there is now a transition region where we find Bloch domain walls ($\alpha = 90°$, dictated by the initial conditions of the simulations), in agreement with our

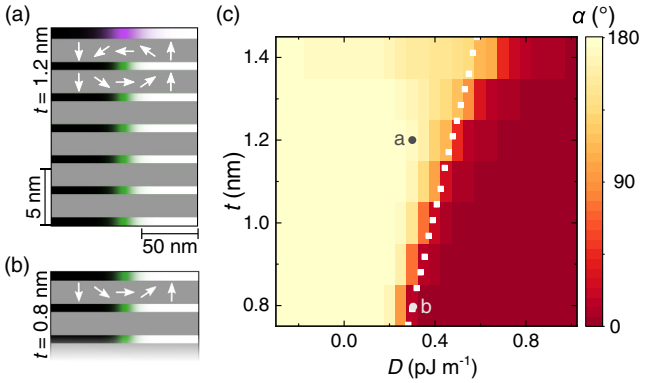

FIG. 3. (a),(b) Result of a micromagnetic simulation with $D = 0.3$ pJ m^{-1} for $t = 1.2$ (a) and $t = 0.8$ nm (b). The arrows indicate the magnetization direction of the layer above. For the colors, see Fig. 1(b). (c) Phase diagram for the domain-wall angle α [Fig. 1(c)] in the top CoB layer from micromagnetics as a function of D and t with $J = 0$ mJ m^{-2}. Also indicated is the transition line from CW to CCW from Fig. 2(c) and the location of the simulations shown in (a)–(b).

experimental findings at 1.1 nm (see Fig. 1). As indicated by the white dots in Fig. 3(c), where we show the transition from CW to CCW from Fig. 2(c), the behavior matches quantitatively with the analytical calculations of Fig. 2(c). As a function of t we find slight deviations, which are attributed to a variation in domain-wall width as we demonstrate in the Supplemental Material [23], Sec. IV. In Sec. VIII of Ref. [23] we further demonstrate that the experimentally determined domain-wall width also matches the domain-wall width extracted from micromagnetic simulations and that it depends on the CoB thickness t as expected. Similar simulations as a function of J and t can be found in Supplemental Material [23], Sec. VII, where we also find excellent agreement between the analytical calculations and the micromagnetic simulations.

As we have shown, the investigated system can be interpreted using a very elementary model that includes all important physical parameters. As similar layer stacks are extremely relevant because they host skyrmions at room temperature [5,15,18,19], we demonstrate a simple model system to investigate the contributions to the chirality for these systems. We establish the role of dipolar interactions in this Letter. Although the mechanism demonstrated here is quite general, the thickness at which this crossover happens depends critically on the balance between the stray fields and the DMI. In other words, by varying the CoB composition one could increase (decrease) M_s, and thus the stray fields, shifting the transition region to lower (higher) thicknesses. Furthermore, this system can also be used for a thorough investigation into the role of the RKKY interaction for the chirality in these systems. Moreover, these mechanisms can be used to tailor the chirality in these stacks. For example, for magnetic racetrack applications

where a uniform chirality of domain walls and skyrmions is preferred we propose two ways to facilitate this [8–10]. We can vary the thickness of the magnetic layers across the stack to alter the competition between the DMI and dipolar interactions on a layer-by-layer basis to modify the position of the transition between the two Néel caps. Second, we can introduce a significant RKKY coupling by modifying the thickness of both Pt and Ir on a sub-nm scale (see Supplemental Material [23], Sec. VI). By including ferromagnetic RKKY interaction we can make the energy cost for the formation of Néel caps prohibitively high, leading to a uniform chirality determined by the DMI. More generally speaking, the case of antiferromagnetic ($J < 0$) RKKY interaction is potentially even more interesting, as even without DMI the domain and domain-wall behavior is very rich [40,41]. Additionally, the method and model system demonstrated here can be extended to further the understanding of the role of chirality in metastable skyrmions towards data storage applications [9,10,13].

Concluding, by varying the topmost magnetic layer thickness we can tune the relative strength of the DMI with respect to the dipolar coupling which leads to a reversal of the domain-wall chirality. This reversal of the domain-wall chirality was imaged directly using an *in situ* SEMPA. We believe this to be the first direct demonstration of this competition in the determination of domain-wall chirality.

This work is part of the research programme of the Foundation for Fundamental Research on Matter (FOM), which is part of the Netherlands Organisation for Scientific Research (NWO). We acknowledge financial support by the DFG within SFB 668. R. A. D. also acknowledges the support of the European Research Council.

*j.lucassen@tue.nl

[1] M. Bode, M. Heide, K. von Bergmann, P. Ferriani, S. Heinze, G. Bihlmayer, A. Kubetzka, O. Pietzsch, S. Blügel, and R. Wiesendanger, Nature (London) **447**, 190 (2007).
[2] K.-S. Ryu, L. Thomas, S.-H. Yang, and S. Parkin, Nat. Nanotechnol. **8**, 527 (2013).
[3] S. Emori, U. Bauer, S.-M. Ahn, E. Martinez, and G. S. D. Beach, Nat. Mater. **12**, 611 (2013).
[4] A. N. Bogdanov and U. K. Rößler, Phys. Rev. Lett. **87**, 037203 (2001).
[5] K. Everschor-Sitte, J. Masell, R. M. Reeve, and M. Kläui, J. Appl. Phys. **124**, 240901 (2018).
[6] A. Fert, N. Reyren, and V. Cros, Nat. Rev. Mater. **2**, 17031 (2017).
[7] A. Fert, V. Cros, and J. Sampaio, Nat. Nanotechnol. **8**, 152 (2013).
[8] W. Legrand, J.-Y. Chauleau, D. Maccariello, N. Reyren, S. Collin, K. Bouzehouane, N. Jaouen, V. Cros, and A. Fert, Sci. Adv. **4**, eaat0415 (2018).
[9] I. Lemesh and G. S. D. Beach, Phys. Rev. B **98**, 104402 (2018).
[10] W. Legrand, N. Ronceray, N. Reyren, D. Maccariello, V. Cros, and A. Fert, Phys. Rev. Applied **10**, 064042 (2018).
[11] M. Heide, G. Bihlmayer, and S. Blügel, Phys. Rev. B **78**, 140403(R) (2008).
[12] N. Nagaosa and Y. Tokura, Nat. Nanotechnol. **8**, 899 (2013).
[13] Y. Dovzhenko, F. Casola, S. Schlotter, T. X. Zhou, F. Büttner, R. L. Walsworth, G. S. D. Beach, and A. Yacoby, Nat. Commun. **9**, 2712 (2018).
[14] K. Fallon, S. McVitie, W. Legrand, F. Ajejas, D. Maccariello, S. Collin, V. Cros, and N. Reyren, arXiv:1901.03652.
[15] A. Hrabec, J. Sampaio, M. Belmeguenai, I. Gross, R. Weil, S. M. Chérif, A. Stashkevich, V. Jacques, A. Thiaville, and S. Rohart, Nat. Commun. **8**, 15765 (2017).
[16] A. Hubert and R. Schäfer, *Magnetic Domains: The Analysis of Magnetic Microstructures*, 1st ed. (Springer-Verlag Berlin Heidelberg, New York, 1998), pp 240–241.
[17] A. Malozemoff and J. Slonczewski, *Magnetic Domain Walls in Bubble Materials*, Applied Solid State Science: Supplement (Academic Press, New York, 1979).
[18] C. Moreau-Luchaire, C. Moutafis, N. Reyren, J. Sampaio, C. A. F. Vaz, N. Van Horne, K. Bouzehouane, K. Garcia, C. Deranlot, P. Warnicke, P. Wohlhüter, J.-M. George, M. Weigand, J. Raabe, V. Cros, and A. Fert, Nat. Nanotechnol. **11**, 444 (2016).
[19] S. Woo, K. Litzius, B. Krüger, M.-Y. Im, L. Caretta, K. Richter, M. Mann, A. Krone, R. M. Reeve, M. Weigand, P. Agrawal, I. Lemesh, M.-A. Mawass, P. Fischer, M. Kläui, and G. S. D. Beach, Nat. Mater. **15**, 501 (2016).
[20] S. A. Montoya, S. Couture, J. J. Chess, J. C. T. Lee, N. Kent, D. Henze, S. K. Sinha, M.-Y. Im, S. D. Kevan, P. Fischer, B. J. McMorran, V. Lomakin, S. Roy, and E. E. Fullerton, Phys. Rev. B **95**, 024415 (2017).
[21] H. Oepen and H. Hopster, *Sempa studies of thin films, structures, and exchange coupled layers, in Magnetic Microscopy of Nanostructures*, edited by H. Hopster and H. P. Oepen (Springer Berlin Heidelberg, Berlin, Heidelberg, 2005), pp. 137–167; J. Unguris, *Scanning electron microscopy with polarization analysis (sempa) and its applications, in Experimental Methods in the Physical Sciences*, Vol. 36, edited by M. De Graef and Y. Zhu (Academic Press, San Diego, 2001), pp. 167–193.
[22] D.-S. Han, K. Lee, J.-P. Hanke, Y. Mokrousov, K.-W. Kim, W. Yoo, Y. L. W. van Hees, T.-W. Kim, R. Lavrijsen, C.-Y. You, H. J. M. Swagten, M.-H. Jung, and M. Kläui, Nat. Mater. **18**, 703 (2019); A. Fernández-Pacheco, E. Vedmedenko, F. Ummelen, R. Mansell, D. Petit, and R. P. Cowburn, Nat. Mater. **18**, 679 (2019).
[23] See Supplemental Material at http://link.aps.org/supplemental/10.1103/PhysRevLett.123.157201 for (I) experimental details, (II) supporting SEMPA measurements, (III) details on micromagnetic simulations, (IV) details on model calculations, (V) histogram width analysis, (VI) experimental RKKY coupling, (VII) simulations on RKKY coupling, and (VIII) experimental domain wall widths. It additionally includes Refs. [24–30].
[24] R. Frömter, H. Stillrich, C. Menk, and H. P. Oepen, Phys. Rev. Lett. **100**, 207202 (2008).

[25] E. C. Corredor, S. Kuhrau, F. Kloodt-Twesten, R. Frömter, and H. P. Oepen, Phys. Rev. B **96**, 060410(R) (2017).
[26] A. Vansteenkiste, J. Leliaert, M. Dvornik, M. Helsen, F. Garcia-Sanchez, and B. Van Waeyenberge, AIP Adv. **4**, 107133 (2014).
[27] M. T. Johnson, P. J. H. Bloemen, F. J. A. den Broeder, and J. J. de Vries, Rep. Prog. Phys. **59**, 1409 (1996).
[28] C. Eyrich, A. Zamani, W. Huttema, M. Arora, D. Harrison, F. Rashidi, D. Broun, B. Heinrich, O. Mryasov, M. Ahlberg, O. Karis, P. E. Jönsson, M. From, X. Zhu, and E. Girt, Phys. Rev. B **90**, 235408 (2014); P. J. Metaxas, J. P. Jamet, A. Mougin, M. Cormier, J. Ferré, V. Baltz, B. Rodmacq, B. Dieny, and R. L. Stamps, Phys. Rev. Lett. **99**, 217208 (2007).
[29] J. D. Clercq, J. Leliaert, and B. V. Waeyenberge, J. Phys. D **50**, 425002 (2017).
[30] P. Bruno, Phys. Rev. B **52**, 411 (1995).
[31] J. Lucassen, F. Kloodt-Twesten, R. Frömter, H. P. Oepen, R. A. Duine, H. J. M. Swagten, B. Koopmans, and R. Lavrijsen, Appl. Phys. Lett. **111**, 132403 (2017).
[32] G. Chen, T. Ma, A. T. N'Diaye, H. Kwon, C. Won, Y. Wu, and A. K. Schmid, Nat. Commun. **4**, 2671 (2013).
[33] R. Frömter, S. Hankemeier, H. P. Oepen, and J. Kirschner, Rev. Sci. Instrum. **82**, 033704 (2011).
[34] There is also a decreasing domain size with increasing CoB thickness which we ascribe to an as-deposited state that is not the ground domain state.
[35] S. S. P. Parkin, Phys. Rev. Lett. **67**, 3598 (1991).
[36] R. Lavrijsen, A. Fernández-Pacheco, D. Petit, R. Mansell, J. H. Lee, and R. P. Cowburn, Appl. Phys. Lett. **100**, 052411 (2012).
[37] I. Lemesh, F. Büttner, and G. S. D. Beach, Phys. Rev. B **95**, 174423 (2017).
[38] Value is the mean and the error bar is half the width of the rectangle indicated in Fig. 2(c).
[39] X. Ma, G. Yu, C. Tang, X. Li, C. He, J. Shi, K. L. Wang, and X. Li, Phys. Rev. Lett. **120**, 157204 (2018); S. Tacchi, R. E. Troncoso, M. Ahlberg, G. Gubbiotti, M. Madami, J. Åkerman, and P. Landeros, Phys. Rev. Lett. **118**, 147201 (2017); D.-S. Han, N.-H. Kim, J.-S. Kim, Y. Yin, J.-W. Koo, J. Cho, S. Lee, M. Kläui, H. J. M. Swagten, B. Koopmans, and C.-Y. You, Nano Lett. **16**, 4438 (2016); S. Finizio, S. Wintz, K. Zeissler, A. V. Sadovnikov, S. Mayr, S. A. Nikitov, C. H. Marrows, and J. Raabe, Nano Lett. **19**, 375 (2019).
[40] O. Hellwig, A. Berger, J. B. Kortright, and E. E. Fullerton, J. Magn. Magn. Mater. **319**, 13 (2007).
[41] R. Lavrijsen, J.-H. Lee, A. Fernández-Pacheco, D. C. M. C. Petit, R. Mansell, and R. P. Cowburn, Nature (London) **493**, 647 (2013).